PHYSICAL REVIEW B

SOLID STATE

THIRD SERIES, VOL. 1, NO. 12 15 JUNE 1970

Fermi Surface of Zinc: Radio-Frequency Size Effect*

O. L. Steenhaut† and R. G. Goodrich

Department of Physics and Astronomy, Louisiana State University, Baton Rouge, Louisiana 70803

(Received 26 November 1969)

The Fermi surface of zinc is determined from calipers obtained through rf size-effect measurements. The 6- to 8-MHz rf measurements were performed at 1.2 °K on high-purity monocrystals of zinc approximately 0.5 mm in thickness. The Fermi surface was calipered using samples whose normals to the surfaces were parallel to one of the three principal symmetry directions, [0001], [10$\bar{1}$0], and [11$\bar{2}$0], with magnetic field rotations in the plane of the sample. Calipers are assigned to definite orbits on the first- and second-band hole surfaces and the third-band electron surface. The third-band electron "lens" is found to be smooth and round with a major diameter of 1.737 Å^{-1} and varying less than 0.5% in the basal plane. The minor diameter has a caliper of 0.556 Å^{-1}. Calipers are given for the first-band hole surface and the spin-orbit-induced gaps between the first and second bands are discussed. The second-band hole surface is discussed in detail with the assignment of 30 series of calipers to definite orbits on this sheet of the Fermi surface. Both the first and second bands of holes are found to have considerably smaller cross sections than predicted by the single-orthogonalized-plane-wave construction. Detailed comparisons to a recent pseudopotential calculation of the energy bands and the Fermi surface are made. No calipers were observed that could be assigned to the third-band "stars" or the fourth-band electron "cigars."

I. INTRODUCTION

In the past few years, the Fermi surface (FS) of zinc has been studied extensively by many investigators.[1] The results of these experiments have been given varied and often conflicting interpretations until an accurate pseudopotential calculation by Stark and Falicov[2] (SF) resolved many of the conflicts. The purpose of the present investigation was to experimentally obtain extensive and detailed dimensions of the Zn FS and to make comparisons with the dimensions calculated by SF. In general, the agreement between the present results and the SF calculation is found to be excellent (approximately 1%), making the topology of the FS of Zn as well known as any metal.

The FS dimensions measured in this experiment were obtained from radio-frequency size effect (rfse) measurements. Except for a few improvements which make the FS determinations more accurate, the experimental technique has been described in detail earlier.[3] Briefly, the experiment consists of measuring the rf surface impedance of a thin slab of the sample as a function of magnetic field applied in the plane of the slab. Discontinuities in the surface impedance (R) are observed at values of the applied magnetic field which allow extremal electronic orbit sizes to span the sample thickness. FS dimensions can then be obtained through the relation

$$k_c = 0.015194Hd\ , \qquad (1)$$

where H is the value of the field at the discontinuity in gauss, d is the thickness of the sample in mm, and k_c is an extremal distance across the FS in Å^{-1}.

In the sections which follow, the important aspects of the experimental apparatus and procedure are described, the results presented, and a complete FS description obtained from these results is given. Finally, a comparison to the FS obtained by SF is made and a brief discussion of the line shapes is given.

Copyright © 1970 by The American Physical Society.

II. EXPERIMENTAL DETAIL

The samples on which the measurements in this experiment were performed were cut from a zone refined bar of Zn obtained from Cominco Products Incorporated (quoted purity: 99.9999%). The 1-kg bar was etched in a 94% HNO_3 and 6% chromic-acid solution which made the boundaries between several large monocrystals easily visible. One of these crystals was selected and cut from the bar by spark erosion. Samples to be used in the measurements were then oriented, cut, and planed thin in the manner described in Ref. 3. In order to obtain strain-free samples for field rotations in the (0001) plane, it was necessary to perform the spark-erosion cutting and planing at temperatures above room temperature. This was accomplished by immersing the sample and goniometer in a small container of Primol 355 (Humble Oil and Refining Company) which was heated to 250 °C with an immersion heater and, in addition, the bath was continuously stirred during the cutting procedure to avoid thermal gradients across the sample. Samples cut and planed at 250 °C showed no indication of strain on back-reflection pictures after etching, whereas samples planed at room temperature always resulted in distorted x-ray spots.

After the cutting and thinning procedure was completed, the surfaces of the samples were cleaned and a small amount of residual surface strain due to the spark cutting was removed by dipping the samples in concentrated HNO_3 for 1 sec. An equally satisfactory procedure for preparing the surfaces was found to be to lap each surface on a microscope slide immersed in a 1% solution of HNO_3 in alcohol. The finished samples were always checked to assure that the final orientation was correct and was always found to be within less than $\pm 1^\circ$ of the required orientation while exhibiting no discernable strain on the back-reflection pictures.

The average thickness of each sample was determined by measuring the area of the face of the slab and weighing the sample in the manner described by JGF. The thickness determinations were made on large slabs from which the final sample was cut. The low-temperature thickness used in calculating the k_c values was then determined using the thermal expansion data for Zn given by the National Bureau of Standards.[4] The sample holder and rf-coil arrangement was the same as given in JGF and all FS measurements were performed at 1.1 °K obtained by pumping on the helium bath.

The electronic detection system and magnetic control used here were modified from that used by JGF to improve the accuracy with which the FS could be determined. A calculation of the rfse line shape by Juras[5] shows that the point on the rather complicated line shape which gives the correct caliper value is the point of maximum slope preceding the first peak in the dR/dH-versus-H curve. This point can be easily determined by recording d^2R/dH^2 versus H and the electronic detection system was modified for this purpose. The resulting detection circuitry is shown in Fig. 1. A harmonic generator is inserted in the reference signal side of the phase detector so that the system is tuned to twice the field-modulation frequency. This arrangement is standard and allows d^2R/dH^2 to be plotted. The harmonic generator and rejection filter can be switched out of the circuit to record dR/dH when desired.

In most FS determinations from rfse measurements on high-purity metals, highly stabilized and programmable magnetic fields in the range 0–1000 G are required. A 4-in.-diam pole face iron-core electromagnet with a 2-in. gap is used in this laboratory for these measurements and the field-control system for this magnet was specially designed and built to make accurate rfse measurements. The system allows the field to be set at any value between −1000 and +1000 G and field sweeps of 2 up to 1000 G to be made starting from the preset field. Since magnetic field modulation at 50 Hz is used in the detection of the rfse and high modulation amplitudes are not required, the field is modulated directly through the dc supply for the magnet.

The over-all reproducibility of this electronic system and sample-thickness measuring technique is 0.5% as determined by caliper values obtained for the same orbit on different samples.

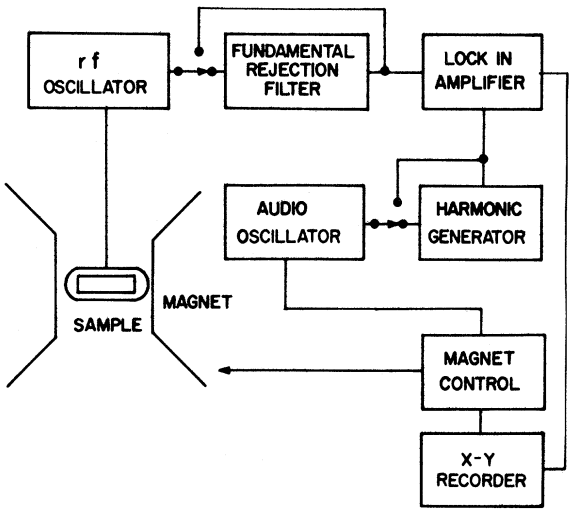

FIG. 1. Block diagram of rfse detection system for the detection of d^2R/dH^2.

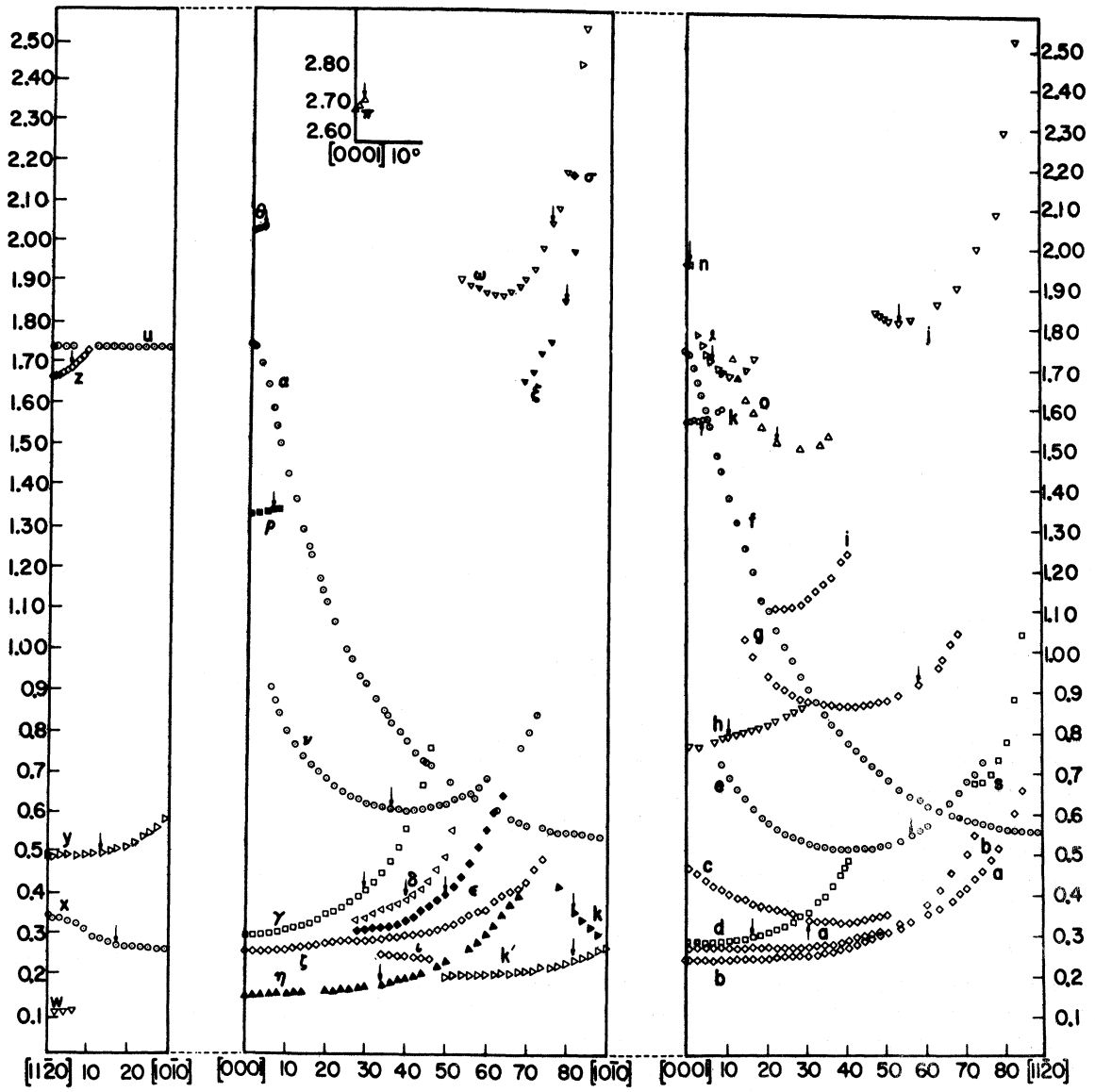

FIG. 2. Caliper values for $\vec{n} \parallel [0001]$, $\vec{n} \parallel [10\bar{1}0]$, and $\vec{n} \parallel [11\bar{2}0]$ in Zn. The arrows refer to the angles at which the calipers are indicated in Figs. 5-7.

III. EXPERIMENTAL RESULTS

Data were obtained for field rotations in three symmetry planes. Thus, samples were used having the normal to the face of the slab, $\vec{n}$, parallel to the [0001], [10$\bar{1}$0], and [11$\bar{2}$0] axes. A general feature of all the data on Zn is that all of the rfse lines are weaker than those previously observed in Cd,[3] even though the sample purity, state of strain, and the temperature dependence of the line intensity were approximately the same. In addition, many more broken orbits are observed in Zn than were observed in Cd and these type orbits depend on sharp corners of the FS in order to be detected. This may indicate that the FS is much sharper in Zn than in Cd.

All of the caliper values computed from the observed data are plotted in Fig. 2. The calipers which could be definitely assigned as being due to the addition of two orbits are not shown on this figure. The values given in Fig. 2 were determined through Eq. (1) from the field at which the first peak in the second derivative curve occurred. The values are reproducible to within ± 0.5% between different samples and all of them can be assigned to orbits on the Zn FS.

The data for $\vec{n} \parallel [0001]$ were recorded by rotating the magnet in 1° steps over a 45° range that cov-

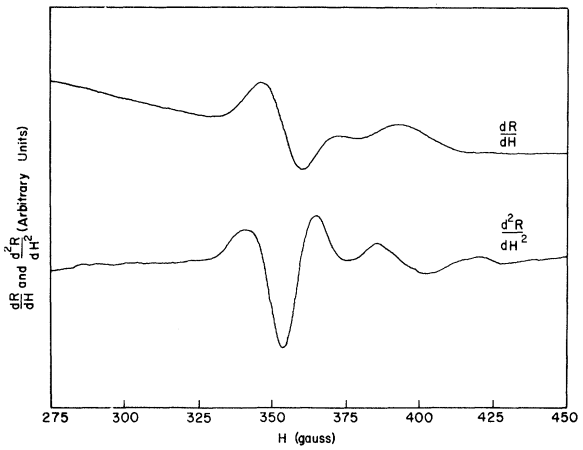

FIG. 3. First- and second-derivative recorder tracings of the lens caliper for $\vec{n} \| [0001]$.

ered two axes, $[10\bar{1}0]$ and $[11\bar{2}0]$. Recorder traces obtained in this orientation for both first derivative and second derivative detection are shown in Fig. 3. The signal-to-noise ratio was always very poor for this orientation and degraded strongly when the sample was cycled between 4.2 and 300°K. This behavior was observed on four different samples cut from different single crystals and was independent of sample size, rf frequency, and method of surface preparation. In this orientation there was a strong field-dependent background signal extending over the entire field range investigated which added to the difficulty in observing the size-effect peaks.

IV. DATA ANALYSIS AND CALIPER ASSIGNMENT

Throughout this discussion the same definition of caliper is used as was defined by JGF. That is, an extremal caliper is defined as a vector quantity in k space which is in the direction of $\pm \vec{n} \times \vec{H}$ and has a magnitude equal to the length of the line segment formed by projecting an extremal orbit (in k space) onto a plane perpendicular to $\vec{n}$. Since the rfse always obtains values of extremal calipers, the term caliper will be taken to mean extremal caliper throughout.

The Brillouin zone (BZ) for zinc is shown in Fig. 4 along with the zone dimensions for reference. The results of the calculation of SF show that there are only four sheets of the FS in Zn. The electron surfaces are in the third zone and in the repeated zone scheme form a large portion centered at the Γ point (lens) and an extremely small pocket at the K point (needles). The first band crosses the Fermi level near the H point (caps) and the second band gives rise to the complicated, multiply connected surface known as the "monster." The single-orthogonal-plane-wave construction of the Zn

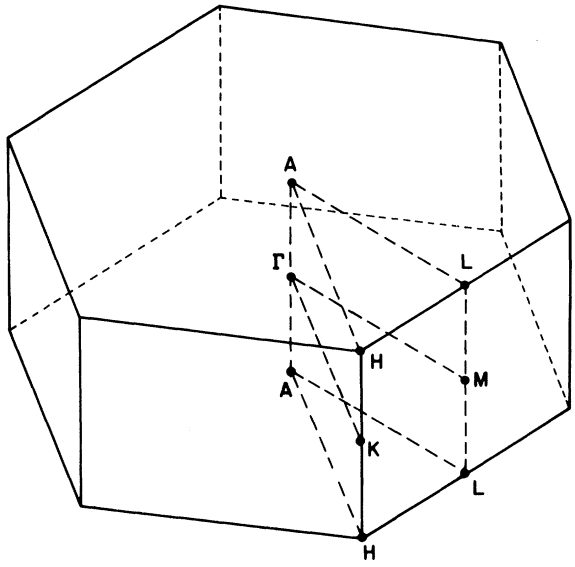

FIG. 4. The Brillouin zone for Zn. The dimensions of the zone are $|\Gamma A| = 0.64610$ Å^{-1}, $|\Gamma M| = 1.36402$ Å^{-1}, and $|\Gamma K| = 1.574919$ Å^{-1}.

FS predicts two additional sheets of the surface (third-band stars and fourth-band cigars), but the calculation of SF has shown these portions of the bands to be above the Fermi level and no data is presented here to contradict this conclusion.

A. Third-Band Electrons

The assignment of caliper series u, α, and f in Fig. 2 to the third-band lens was immediately obvious. In all three orientations, the plane of the orbit giving rise to this caliper passes through the Γ point and all caliper values have their midpoint on Γ. The lens has a circular cross section in the ΓMK plane with a diameter of 1.737 ± 0.0015 Å^{-1} with the error representing the maximum deviation found at all field directions and among four samples with $\vec{n} \| [0001]$.

From the data on the lens in the $\vec{n} \| [10\bar{1}0]$ and $\vec{n} \| [11\bar{2}0]$ orientations, series α and series f, it is seen that it is quite smooth and only slightly

TABLE I. Comparison of measured cross-sectional areas of the lens in zinc. All areas measured in Å^{-2}.

Plane	ΓKM	ΓAHK	ΓALM
Thorsen, Valby, and Joseph[a]	2.39	•••	•••
Stark[b]	2.34	0.693	0.693
Present investigation	2.37	0.692	0.689

[a]See Ref. 1.

[b]R. W. Stark (private communication and to be published).

rounded on the edges. Since all of these caliper values lie in the ΓAHK and ΓALM planes, respectively, the cross-sectional areas of the lens in these planes could be calculated directly on an electronic computer. The results of these area calculations plus the area in the ΓKM plane (area $= \frac{1}{4}\pi k_c^2$) are presented in Table I and compared with direct measurements of the same areas by the de Haas–van Alphen (dHvA) effect. It is seen that the agreement for the ΓAHK and the ΓALM planes is particularly good and the ΓKM plane gives slightly more than 1% difference. This is within our estimated error of 0.5% for the caliper values which becomes 1% for the areas.

The second portion of the third-band electron surface is the needle located at the K point. No calipers for the needles were observed in the present investigation. This, however, is not surprising because the expected field for observing the needles is between 1 and 10 G for the sample thicknesses used. In this field range, there is an extremely steep background slope in the traces which could not be entirely removed even when recording d^4R/dH^4. In addition, the iron magnet used demagnetizes inhomogenously giving rise to a very inhomogenous field below 15 G. A search for the needles was performed on one of the $\hat{n} \parallel [11\bar{2}0]$ samples, but the results were not considered reliable.

B. Second-Band Hole Surface

There are two methods by which the second-zone hole surface (monster) in Zn can be described. First, the attitude can be taken that the monster is a single surface described by a ring centered at the Γ point with branches extending toward the corner of the zone. Second, because of inversion symmetry through Γ one can consider it as a set of two trifoliate posts per BZ centered along the KH line in the repeated zone scheme and connected together in the ΓALM planes. In both of these descriptions, the surface is multiply connected in the [0001] direction. The first of these approaches is the one always taken in beryllium since this surface is not connected in the [0001] direction, the second is usually taken in cadmium since this surface is not connected in the ΓALM planes, and these two cases represent the extremes of divalent hexagonal metals. The Zn surface is connected both in the [0001] direction and in the ΓALM planes, thus a combination of these two approaches is taken here. The surface will be considered to be a ring entirely contained in one BZ but, because of the connections, the repeated zone scheme will be required to assign some of the calipers and some of the calipers will be degenerate because of the inversion symmetry through the Γ point. In Fig. 5, the solid line cross section is the ring surface in the ΓMK plane (the connection regions in the ΓAML planes are called the "arms"), the cross-hatched triangle sections are in the AHL plane ("neck"), and the shaded portions are the extremities of the surface between these two planes (i.e., the shadow of the surface projected onto the ΓMK plane).

Because of the lack of inversion symmetry for each trifoliate post of the surface, the monster has no central calipers for $\hat{n} \parallel [0001]$ or $\hat{n} \parallel [10\bar{1}0]$ except for those orbits which include the Γ point in their plane. That is, there are no series of calipers that have a common fixed point on a symmetry point or line in the BZ for these orientations other than those traversing the complete connected ring.

There are several different types of extremal calipers that can give rise to an rfse peak: (1) calipers due to orbits having a true maximal or minimal extent in the $\hat{n} \times \hat{H}$ direction, (2) calipers due to truncated orbits which are orbits in planes perpendicular to $\hat{H}$ that increase in extent until they reach a point on the surface at which they no longer exist in the same form (these calipers are still classified as extremal calipers even though they are not extremal in the same sense as in case 1 and case 3), and (3) calipers due to broken orbits which are obtained between turning points on an orbit. Orbits of the above types can be either open or closed.

Open orbits existing on the monster with $\hat{H}$ in the (0001) plane have their extremities perpendicular to [0001] in the AHL and ΓMK planes. Thus, open or-

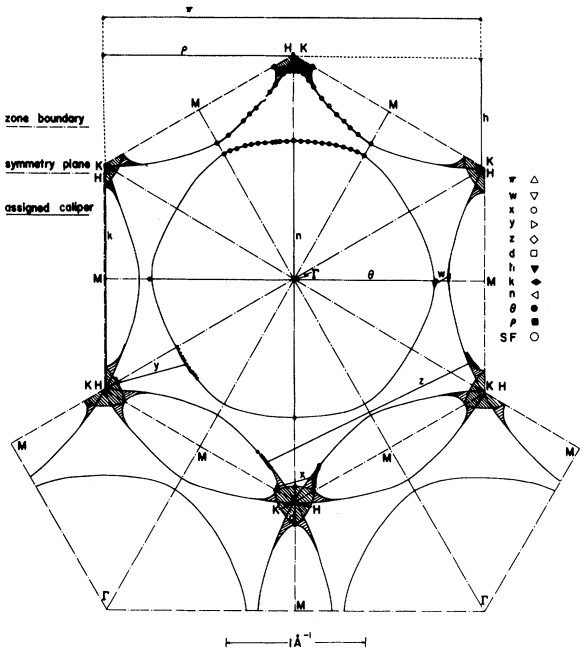

FIG. 5. Projection of the second-zone Zn FS onto the ΓKM plane.

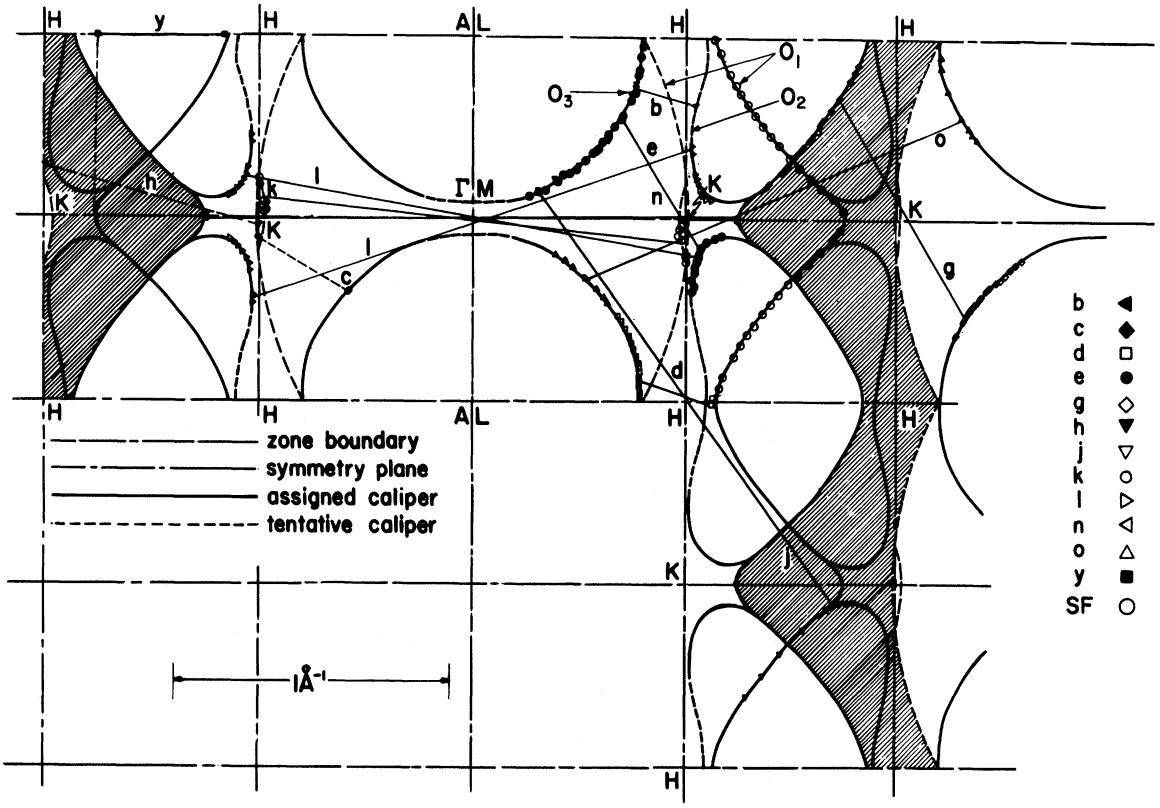

FIG. 6. Projection of the second-zone Zn FS onto the ΓAHK plane. The shaded section corresponds to the true FS cross section in the ΓAHK plane.

bits on the monster caliper the difference in extent of the surface in these two planes. These orbits have a shape similar to the cross section of the monster given by the points from the calculation of SF and labeled O_1 in Fig. 6. The projection of the monster on the ΓAHK plane was obtained from the $\vec{n} \parallel [10\bar{1}0]$ data and is shown in Fig. 6. The heavy lines indicate the portions of the surface lying in the ΓAHK plane and the lighter lines are the extremities of the surface between adjacent ΓAHK planes projected onto a ΓAHK plane. The principal calipers obtained with $\vec{n} \parallel [11\bar{2}0]$ are central in the sense that the corresponding orbits are symmetrical relative to either the ΓK or AH lines. Noncentral calipers are obtained from truncated orbits for this orientation. The projection of the extremities of the monster onto the ΓALM plane is shown in Fig. 7.

As a starting point for the assignment of calipers to the FS, the points on the FS obtained from the pseudopotential calculation of SF were plotted and then modifications were made to give a completely self-consistent result with extremal calipers in all directions fitting the data. The calculated points used here are from the nonlocal pseudopotential calculation, but without spin-orbit coupling (soc) included. As will be seen, this only causes a measurable discrepancy near the K point and on the neck and arms of the monster. The calculated points are shown in Figs. 5 and 6 as large open circles.

Series z was easily identified as being produced by a dogbone-shaped orbit connecting two nonadjacent diagonal arms. This series of calipers determines the outline of the extremities of the monster between the ΓKM and the AHL planes projected onto the ΓKM plane. Further calipering of these extremities is obtained from the x series which is a minimum caliper due to a closed orbit. Since neither of these two calipers is central, the outline was constructed self-consistently until at each angle both of the measured caliper series were extremal and of the correct value. Series y is due to the open orbit in the [0001] direction and was found to fit the calculated values to within 1%. This cross section is further confirmed by the n caliper due to an orbit around the inside ring of the monster for $\vec{H} \parallel [0001]$ and $\vec{n} \parallel [10\bar{1}0]$ which also fits the distance from Γ to the monster in the ΓKM plane to better than 1%.

Series w for $\vec{n} \parallel [0001]$ is due to an orbit around

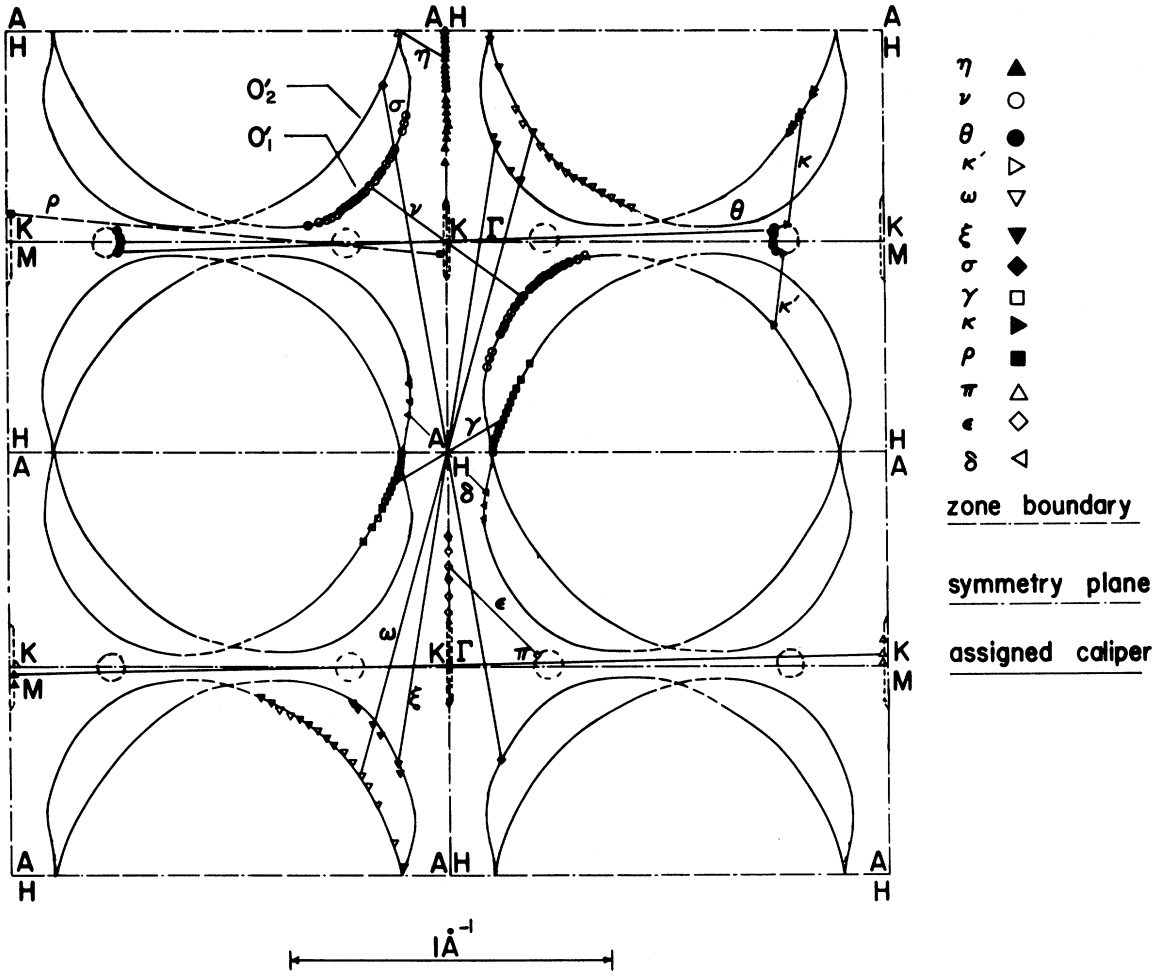

FIG. 7. Projection of the second-zone Zn FS onto the ΓALM plane.

the connecting arm. The signal due to this caliper was very weak. Since it is a small value, it is observed at low fields where the background slope is steep and was only observable when recording d^2R/dH^2 because of the reduction of the background. The calipers obtained from this series are slightly smaller than those predicted by SF. This is again confirmed by the θ series for $\vec{H}\|[0001]$ and $\vec{n}\|[11\bar{2}0]$ which is due to the inside monster orbit and is slightly larger than calculated.

Several other calipers were observed for $\vec{H}\|[0001]$ and $\vec{n}\|[10\bar{1}0]$ or $\vec{n}\|[11\bar{2}0]$ which give information about the surface in the ΓKM and AHL planes. Series ρ, π, h, and k caliper between the points on the surface in the ΓKM plane nearest the K point of the BZ. All of these calipers arise from orbits around the outside ring of the monster. Only one of them, however, is due to a complete orbit, π; the remainder arise from broken orbits at the sharp turning points. It is found that these calipers consistently give about 1% smaller values than predicted by SF meaning probably that these corners near K are slightly rounded by the soc.

Since most of the calipers obtained for $\vec{n}\|[10\bar{1}0]$ are noncentral, the projection of the surface on the ΓAHK plane (Fig. 6) was constructed self-consistently starting with one outline from the calculation of SF. Series n corresponds to central orbits around the inside ring of the monster and gives calipers which reproduce the SF outline over a small angular range near the ΓMK plane. The orbits giving rise to the n series break into orbits giving rise to the l series of calipers when the angle between $\vec{H}$ and [0001] becomes larger than 3°. The orbit giving the l series is a dogbone-shaped closed orbit passing across the arms and through the openings near the K point until $\vec{H}$ is directed greater than 11° from [0001]. After 11° the l caliper is obtained from the turning points on a more extended orbit. This assignment is verified by the fact that at 11°

the line shape giving the l series changes drastically. Since the plane of this orbit always passes through the ΓALM mirror plane, it could be plotted with its midpoint on the ΓM line, giving part of the outline labeled O_2 in Fig. 6 directly. The remainder of outline O_2 was constructed from a self-consistent fitting of series b which arises from a broken orbit around the neck. This portion of O_2 can only be tentatively drawn since there is not a second series of calipers with which to check the self-consistent fitting procedure for uniqueness.

The outline indicated as O_3 on Fig. 6 was constructed self-consistently from five different caliper series. The two-zone orbit giving series j and the neck orbit giving series d both have one caliper point on the SF outline (O_1) and the other caliper point on O_3. Caliper series O arises from a rather complicated orbit extending across two arms (and therefore noncentral on the ΓM line) and through two openings near the K points close to the caliper points. Series c is due to a truncated orbit and extends from the top of the opening near K to O_3. Series e calipers between the O_2 and O_3 outline and confirms both of their constructions. The O_3 outline is constructed such that every measured caliper in these five series is extremal and has the correct magnitude at each angle. This completes the definitely assigned outline of the monster projection onto the ΓAHK plane except for points near the K point and along outline O_1' for which no calipers are obtained.

From the angular ranges of series l, e, and h the extent of the opening along the KH line can be deduced. Series e disappears sharply when they no longer pass through this opening and the h and l series undergo a change in intensity and line shape as they change from closed to broken orbits. All of these series give a distance of 0.130 ± 0.005 Å^{-1} for the distance from the K point to the point where the second band crosses the HK line of the BZ. The value of $0.135\ \text{Å}^{-1}$ for this distance that was found by Schirber[1] is in excellent agreement with the present determination.

Series i, m, and s are not definitely assigned, although they can be fit on different truncated orbits in the angular range in which they are observed. The remaining caliper series g is somewhat puzzling. No direct orbit of this size exists because of the opening at the K point, but it fits exactly the measured extremal calipers at all angles as it is shown. There are two possibilities for its appearance: (1) Series g arises from the sum of two nonextremal caliper orbits passing through the opening whose sum is an extremal caliper, or (2) series g arises from a magnetic-breakdown orbit through the third-band needles. The first of these conjectures has the drawback that no other series of nonextremal calipers adding to yield an extremal caliper is observed although there are many which might be. The range of magnetic fields over which series g is observed is from 170 to 280 G. This is far below the 2.2-kG breakdown field determined by Higgins and Marcus.[1] The effect of magnetic breakdown on the needles has been observed as low as 1 kG[1] but since the probability of breakdown for this orbit varies as $(1 - e^{-H_0/H})^{n/2}$, where $H_0 = 2.2$kG and $n = 2$, the probability of this orbit occurring at 220 G is $(1 - e^{-0.1}) = 0.095$ or about 10%. The plane of the orbits giving extremal calipers for the g series does not pass through the breakdown points in the ΓKM plane. If the details of the structure in the opening are similar to that found in magnesium,[6] the breakdown field H_0 may be much smaller away from this plane. Again, the size of these calipers relative to the dimensions of the opening prohibits any definitive determination of the angular dependence of the breakdown field from amplitude studies.

The projection of the surface onto the ΓALM plane is shown in Fig. 5, and it was much easier to construct than the other two, because most of the calipers pass through the ΓAHK mirror plane and are therefore central calipers. Caliper series υ is readily assigned as being due to an orbit on one section of the monster passing through the opening near K and out over the body. This series is observed over a 68° range and almost completely determines the outline of this portion of the surface labeled O_1' in Fig. 7. The ξ series is due to a two-zone orbit and calipers the same outline as the υ series. The second portion of the outline, O_2', is obtained from caliper series γ, the neck orbit ω, a two zone orbit ξ, and δ a broken orbit on the neck. In each of these cases, the lines are observed over the full angular range allowed by this construction and disappear at other angles.

The two-zone σ orbit caliper is due to a broken orbit and calipers between the two outlines, O_1' and O_2'. The η orbit is a broken orbit around the neck and the ϵ orbit is a broken orbit from the arms to the sharp turning point near the KH line. Neither of these calipers gives any new information about the outline. The dogbone orbit arising when $\vec{H}$ is near the $[10\bar{1}0]$ axis does not have an extremal caliper in these directions and is not observed. However, extremal calipers are observed from two parts of this orbit. Series k and k' are due to broken portions of the dogbone orbit which do give an extremal caliper for the field near $[10\bar{1}0]$. The line shape is very complicated in this field region for these orientations, but the two peaks giving the k and k' calipers can be determined. Series ι can be fitted on a noncentral truncated orbit around the arms.

The remainder of the calipers obtained in this ori-

entation arise from either complete or broken orbits around the ring network for $\vec{H}$ near [0001]. The θ series is due to the complete orbit around the inside of the monster and gives the outline of the arms in the ΓML plane. As was stated earlier, the arm cross section is found to be slightly smaller than calculated by SF without soc. The π and ρ series are the complete and broken parts of the orbit around the outside of the monster giving the distance between the extremities of the openings near the K points.

C. First-Band Hole Surface

The first-band hole surface (cap) consists of two surfaces per BZ centered at the H point. Except for the connectivity in the KM direction of the monster, the caps have the same symmetry properties as the monster. All of the calipers for this surface can be assigned by considering only one of the two surfaces.

Series a and ζ have been assigned to the caps and the cross sections obtained are shown in Fig. 8. Because of poor signal-to-noise ratios for $\vec{n} \| [0001]$, no calipers were obtained for the caps for $\vec{H}$ rotated in the basal plane. As in the case of the second-zone surface, the calipers obtained for the cap with $\vec{n} \| [11\bar{2}0]$ do not all lie in a plane, and the outline for the ΓAML plane is not a true cross section of the cap, but a profile or projection of the extremities onto the plane. In order to construct the cross section of the cap in the ΓAHK plane, the points shown as circles in Fig. 8 were plotted from

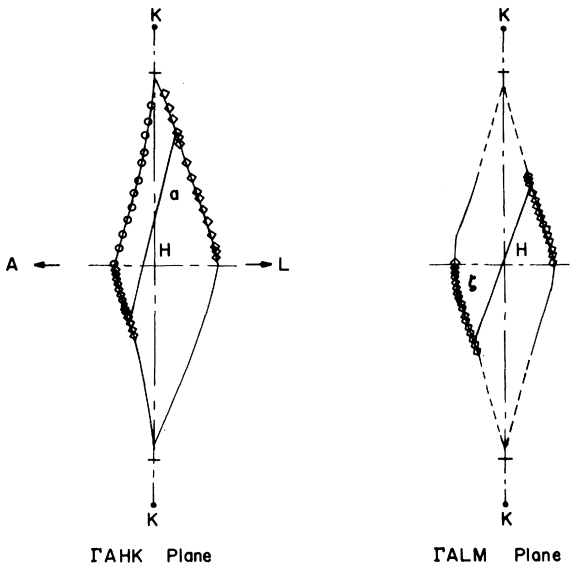

FIG. 8. Projection of the second-zone Zn FS onto the ΓAHK and ΓALM planes. The horizontal lines along the KH line indicate the point at which the second zone crosses this line.

TABLE II. Dimensions of the FS of Zn. All dimensions in $Å^{-1}$.

	Expt	Theory [a]
Third-zone lens		
From Γ in ΓA direction	0.278	
From Γ in ΓK direction	0.869	0.863 [b]
From Γ in ΓM direction	0.869	0.863
Second-zone holes		
From Γ in ΓK direction		
to inside ring	0.978	0.974
near K point	1.547	1.558
From Γ in ΓM direction	1.026	1.018
From A in AH direction	1.467	1.459
Across neck in AH direction	0.282	0.267
Across neck in HL direction	0.285	0.269
Across arms in ΓA direction	~0.08	
Across arms in ΓM direction	~0.08	0.0866
From K on KH line	0.130	
First-zone holes		
Across in AH direction	0.277	0.267
Across in HL direction	0.276	0.269

[a] Values obtained from SF without soc included.

[b] Obtained from area data of Stark (private communication) to which the SF calculation was fit exactly and using an assumed circular orbit.

SF. Then the calipers were put on the outline self-consistently until at each angle an extremal caliper was obtained.

Estimates of the gap between the first and second band caused by soc in the AHL plane can be made from the calipers obtained for the cap and the neck of the monster. The difference in the calipers for $\vec{H} \| [0001]$ and $\vec{n} \| [10\bar{1}0]$ gives the sum of the gaps along the AH line and the LH line. This difference is a maximum of $0.005 \pm 0.001\ Å^{-1}$. The rfse lines from the cap and neck orbits overlap with $\vec{H} \| [0001]$ with the separation between peaks only 0.6 G at 60 G, thus causing the large uncertainty in this value. In the $\vec{n} \| [11\bar{2}0]$ data, the gap is $0.009 \pm 0.0005\ Å^{-1}$ for the projection onto the ΓALM plane. Although the plane in which these caliper values lie is not determined, it should be a close approximation to twice the gap along the HL line showing that the gap along the AH line is probably less than $0.001\ Å^{-1}$.

V. CONCLUSIONS

The experimental numbers obtained in this experiment show very good agreement with the nonlocal pseudopotential calculation of Stark and Falicov[2] without the inclusion of soc. Where disagreement greater than 1% occurs is at points where the soc would have the greatest effect. Some of the results of both the theoretical numbers and the calculated points are given in Table II. It can be seen that except near the H point and along the ΓM line

the agreement is excellent, and the inclusion of soc into the theory would shift calculated values to be in better agreement.

The over-all reproducibility from sample to sample of the caliper values reported here is ± 0.5%. This level of reproducibility is only achieved when accurate average-thickness values are obtained by weighing and the proper point on the rather complex line shapes is chosen. The FS of Zn appears to be very sharp, without a great deal of rounding due to the lattice potential or soc, as evidenced by the large number of turning points or broken orbits observed here.

No calipers which could be assigned to the third-band needles were observed. This is due to the experimental apparatus used, and under proper conditions of low homogenous applied field and thin (~ 0.2 mm) samples, they should be readily observable.

Finally, it is noted that the detailed over-all shape of an rfse line is strongly dependent on the shape of the orbit giving rise to that line. In the case of the lens orbit where the shape is known, the agreement between the observed lines and the line shape given by Juras is good. The point on the complicated line shapes at which the caliper values are calculated does not, however, seem to vary between different line shapes. That is, if one always chooses the first peak in the second derivative of the line, consistent caliper values are obtained.

ACKNOWLEDGMENTS

The authors are indebted to Professor C. G. Grenier for many informative discussions and to Professor L. M. Falicov for providing the points on the FS from the energy-band calculation of SF. Preliminary data on two of the orientations analyzed were taken by J. J. Hill and R. Roth while participating in the National Science Foundation Summer Research Participation for College Teachers. The financial assistance received from the Dr. Charles E. Coates Memorial Fund of the Louisiana State University Foundation donated by George H. Coates for the preparation of this manuscript is gratefully acknowledged.

---

*Work performed under the auspices of the U.S. Atomic Energy Commission and is A.E.C. Report No. ORO-3087-37.

†Present address: Institut de l'Etat pour les Industries Nucléaires, Rue Royale 155, Bruxelles, Belgium.

[1]Some of the more recent investigations are de Haas-van Alphen studies, R. J. Higgins and J. A. Marcus, Phys. Rev. 161, 589 (1967); A. Myers and J. R. Bosnell, Phil. Mag. 13, 1273 (1966); A. S. Joseph and W. L. Gordon, Phys. Rev. 126, 489 (1962); A. E. Thorsen, L. E. Valby, and A. S. Joseph, in *Proceedings of the Ninth International Conference on Low-Temperature Physics, Columbus, Ohio*, 1964, edited by J. G. Daunt *et al.* (Plenum, New York, 1965), p. 867; cyclotron resonance, M. P. Shaw, P. I. Sampath, and T. G. Eck, Phys. Rev. 142, 399 (1966); Yu. P. Gaidukov and I. P. Krechetova, Zh. Eksperim. i Teor. Fiz. Pis'ma v Redaktsiyu 1, 88 (1965) [Soviet Phys. JETP Letters 1, 88 (1965)]; ultrasonic geometric resonance, D. F. Gibbons and L. M. Falicov, Phil. Mag. 8, 177 (1963); galvanomagnetic properties, J. E. Schirber, in *Proceedings of the Ninth International Conference on Low-Temperature Physics, Columbus, Ohio*, 1964, edited by J. G. Daunt *et al.* (Plenum, New York, 1965), p. 863; R. W. Stark, Phys. Rev. 135, A1698 (1964).

[2]R. W. Stark and L. M. Falicov, Phys. Rev. Letters 19, 795 (1967), hereafter referred to as SF.

[3]R. C. Jones, R. G. Goodrich, and L. M. Falicov, Phys. Rev. 174, 672 (1968), hereafter referred to as JGF.

[4]Natl. Bur. Stds. (US) Monograph No. 29 (1961).

[5]G. E. Juras, Phys. Rev. 187, 784 (1969).

[6]J. C. Kimball, R. W. Stark, and F. M. Mueller, Phys. Rev. 162, 600 (1967).